



## A self-powered skin-patch electrochromic biosensor

Sara Santiago-Malagón<sup>a</sup>, Diego Río-Colín<sup>b</sup>, Haniyeh Azizkhani<sup>a</sup>, Miguel Aller-Pellitero<sup>c,d</sup>, Gonzalo Guirado<sup>a</sup>, F. Javier del Campo<sup>c,e,f,\*</sup>

<sup>a</sup> Universitat Autònoma de Barcelona, Bellaterra, Spain

<sup>b</sup> Universidad Del País Vasco, UPV-EHU, Campus de Leioa, Vizcaya, Spain

<sup>c</sup> Instituto de Microelectrónica de Barcelona, IMB-CNM (CSIC), Campus de la Universitat Autònoma de Barcelona, Esfera UAB, 08193, Bellaterra, Barcelona, Spain

<sup>d</sup> Johns Hopkins University School of Medicine, Baltimore, MD, USA

<sup>e</sup> BCMaterials, Basque Center for Materials, Applications and Nanostructures, UPV/EHU Science Park, 48940, Leioa, Spain

<sup>f</sup> IKERBASQUE, Basque Foundation for Science, 48009, Bilbao, Spain



### ARTICLE INFO

**Keywords:**

Electrochromism  
Biosensors  
Self-powered devices  
Wearables  
Lactate biosensor  
Sweat sensing

### ABSTRACT

One of the limitations of many skin-patch wearable sensors today is their dependence on silicon-based electronics, increasing their complexity and unit cost. Self-powered sensors, in combination with electrochromic materials, allow simplifying the construction of these devices, leading to powerful analytical tools that remove the need for external detection systems. This work describes the construction, by screen-printing, of a self-powered electrochromic device that can be adapted for the determination of metabolites in sweat by the naked eye in the form of a 3 × 15 mm colour bar. The device comprises a lactate oxidase and osmium-polymer-based anode connected to a coplanar 3 × 15 mm Prussian Blue, PB, cathode printed over a transparent poly(3,4-ethylenedioxythiophene) polystyrene sulfonate, PEDOT:PSS electrode. An ion-gel composed of Poly(vinylidene fluoride-co-hexafluoropropylene), PVDF-co-HFP, a gelling agent, and ionic liquid 1-Ethyl-3-methylimidazolium trifluoromethanesulfonate, EMIM-Tf, effectively separates the cathode display from the biosensing anode, protecting it from the sample. Despite its cathodic electrochromism, the PEDOT:PSS has a transmission above 90% and does not mask the Prussian Blue colour change because the cathode does not operate below 0 V vs Ag/AgCl at any time. The sensor displays lactate concentrations in the range of 0–10 mM over the length of the electrochromic display, which has a contrast ratio of 1.43. Although full response takes up to 24 min, 85% of the colour change is displayed within 10 min.

### 1. Introduction

Electrochromic materials change optical properties as a function of their oxidation state (Mortimer, 2011; Mortimer et al., 2015). Although they are most commonly used in the fabrication of displays and optoelectronic devices such as anti-glare rearview mirrors, dimmable windows, and electrochromic printed displays (Andersson et al., 2007; Singh et al., 2017), electrochromic materials can also be successfully used in sensing (Aller-Pellitero et al., 2019; Virbickas et al., 2019). The main advantages of electrochromic devices are their relatively low power consumption compared to other technologies, and the ease of fabrication through large-area processes, which also implies low unit costs. Besides, electrochromic sensors simplify device construction by adding the function of information display to the (electrochemical)

sensing event. However, extracting chemical information through electrochromic materials is non-trivial and remains as one of the leading design challenges facing electrochromic (bio)sensors (Aller-Pellitero and del Campo, 2019). In a recent literature survey, we found that electrochromic sensors expressed their analytical results either by changes in colour hue (Liu and Crooks, 2012; Popov et al., 2019; Virbickas et al., 2019; Zhang et al., 2017) or by creating colour gradients (Liana et al., 2015) and coloured bands of different length (Aller-Pellitero and del Campo, 2019). Systems based on colour hue readings require additional instrumentation, such as a spectrophotometer or, in a simpler approach, a smartphone camera, and their corresponding colour analysis software, which correlates colour intensity with an analyte concentration. While this facilitates automation and affords higher sensitivities, it also imposes restrictions on the users and limits the number of possible

\* Corresponding author. Instituto de Microelectrónica de Barcelona, IMB-CNM (CSIC), Campus de la Universitat Autònoma de Barcelona, Esfera UAB, 08193, Bellaterra, Barcelona, Spain.

E-mail address: [Javier.delcampo@bcmaterials.net](mailto:Javier.delcampo@bcmaterials.net) (F.J. del Campo).

form-factors. In contrast, devices based on the translation of chemical information into colour lengths can be read and interpreted by the naked eye without the need for any additional instrumentation (Aller-Pellitero et al., 2017, 2020), providing semi-quantitative results.

Despite their low consumption, power remains an essential issue of electrochromic sensors and biosensors. Most miniaturized dc-power sources used in portable sensors and biosensors, including wearables, are based on batteries (Bandodkar et al., 2020) and fuel cells (Jin et al., 2020; Ortega et al., 2019). These power sources can be turned into self-powered sensors by making their power output proportional to an analyte concentration (Grattieri and Minteer, 2018; Huang et al., 2020; Yu et al., 2019). Most self-powered sensors show limited performance due to the need to produce enough energy to power all the functions around the sensor, such as the display of information or data extraction. Recent progress in low-power electronics and biofuel cell technology (Ruff, 2017; Xiao et al., 2019), have improved the feasibility of these devices. However, manufacturing remains a significant limitation of most self-powered sensors, as most cases involve the heterogeneous integration of discrete and silicon-based components along with the sensor. This makes these disposable devices uneconomical and highly damaging to the environment.

In addition to providing chemical information visually through changes in their optical properties the redox properties of electrochromic materials make them excellent candidates for the construction of self-powered sensors (Yu et al., 2018; Zloczewska et al., 2014), even using screen-printing alone (Aller-Pellitero et al., 2020), which makes these devices amenable to mass production.

In this work, we are taking this concept to a wearable form factor on a flexible substrate. Sweat sensing technologies boomed less than a decade ago, integrating electrochemical sensing into tattoos and skin patches (Heikenfeld et al., 2018; Kim et al., 2011; Rose et al., 2014; Windmiller et al., 2012). Interestingly, despite their considerable evolution (Kim et al., 2019), they face similar manufacturing and cost issues as self-powered sensors: namely connectivity and the heterogeneous integration of discrete electronic components. We believe that multi-functional components (Huang et al., 2020) can hugely simplify the construction of new wearable sensing devices, making their production affordable and appealing. Such multifunctional components, in turn, are enabled by unique combinations of multi-responsive materials (Correia et al., 2020; Mendes-Felipe et al., 2019; Oliveira et al., 2018) and manufacturing techniques. The ultimate aim is to develop new devices that are easy to use without the need for advanced training or complex scientific instrumentation, and that can be easily manufactured by large-area printing methods. Here we present a self-powered lactate skin-patch electrochromic biosensor that can be fully screen-printed and easily read by the naked eye. We show how device design is strongly intertwined with materials and fabrication processes. The choice of the transparent conductor is particularly important as it affects both device construction and performance. This work describes a device where a lactate biosensor anode is coupled to a Prussian Blue (PB) cathode to provide a visual concentration readout. However, changing the enzyme system at the anode will enable the detection of other analytes in sweat or any other media. Because the display is not in direct contact with the sample, the technology can be used with dark or turbid samples as well as clear ones.

## 2. Materials and methods

### 2.1. Reagents and materials

All chemicals and materials were used as received without further purification. **Ion-gel electrolyte:** potassium trifluoromethanesulfonate (KTF) and poly(vinylidene fluoride-co-hexafluoropropylene) (PVDF-co-HFP) were acquired from Sigma-Aldrich (ES), and Ionic liquid 1-Ethyl-3-methylimidazolium trifluoromethanesulfonate (EMIM-Tf) was acquired from Solvionic (FR). **Other reagents:** Potassium hexacyanoferrate (II)

trihydrate, potassium chloride, ferric chloride, and potassium nitrate were purchased from Sigma-Aldrich (ES). A solution of 0.1 M potassium chloride (KCl) from Sigma-Aldrich and 0.05 M phosphate buffer (PBS) pH 7 from Fluka (ES) was selected as aqueous supporting electrolyte for the measurements using the self-powered prototypes. SoftWear 93194 nonwoven double-sided pressure sensitive adhesive (PSA) tape kindly provided by Adhesives Research (IE) was used for attaching the patch to the user's skin. Autotype CT-4 Polyethylene terephthalate, PET, sheets were sourced from MacDermid Autotype (UK).

The fabrication of conventional 3-electrode screen printed electrodes, as well as the lactate biosensor construction, is provided as part of the electronic supplementary information (ESI).

### 2.2. Gel polymer electrolyte

One of the most successful approaches to achieving ion-gel electrolytes with high ionic conductivities is the use of Poly(vinylidene fluoride-co-hexafluoropropylene) (PVDF-co-HFP) ionic liquid-based ion-gels (Dubal et al., 2018). This type of electrolytes, loaded with c. a. 70–80 % wt. of ionic liquid, can reach conductivities up to 1.06 mS cm<sup>-1</sup>, transparencies around 83% of transmittance, and a broad electrochemical window (3.2 V), without losing flexibility or integrity (Santiago et al., 2020). The composition of the gel electrolyte used here, which has an ionic conductivity ca. 4 mS cm<sup>-1</sup>, has been reported recently (Aller-Pellitero et al., 2020), but a short summary will be given for convenience. 0.14 g of the gelling agent, PVDF-co-HFP were dissolved in 0.5 mL acetone while stirring at 2000 rpm at 60 °C for 15–30 min until all the PVDF-co-HFP was dissolved. Note that the mixture yellows out above 70 °C. Next, 50 mg of KTF and 340 μL of ionic liquid were added to the mixture and stirred while heating for up to 1 h in total. Printed layers (3 coats) were measured using a stylus profilometer, yielding values ranging between 10 and 20 μm.

### 2.3. Design and fabrication of the electrochromic biosensor

The fully-printed self-powered electrochromic biosensor concept recently presented in (Aller-Pellitero et al., 2020) has been adapted to take a skin patch form factor, as shown in Fig. 1. In contrast to our previous work, which followed a straightforward coplanar construction, this time biosensor and display must face opposite sides, because the electrochromic material must remain visible to the user through the PET substrate while the biosensor stays in contact with the skin. Also, the biosensor was resized to match the charge on the electrochromic display and ensure readable colour changes within the biosensor dynamic range. We used a 100 μm-thick transparent PET substrate for our experimental work, but we produced a series in 30 micron-PET with the same functionality, but which felt more comfortable to wear. Fig. 1 outlines the fabrication process, where the PET substrate was the top cover of the device, which was thence built "backwards".

First, the substrates were prepared by engraving a series of registration marks in them. These registration marks served as a reference for the subsequent printing and cutting operations. Fig. 1 shows that both indium tin oxide, ITO, (or other forms of transparent mixed tin oxide) and PEDOT:PSS electrodes can be used in the construction. In contrast to PEDOT:PSS, which can be screen-printed and therefore streamline the fabrication process, ITO electrodes require wet-etch patterning (Aller-Pellitero et al., 2017). Although it is easy to make a suitable stencil out of masking vinyl, the process is more tedious and, on top of that, ITO on PET can be heterogeneous and present very variable conductivities even on the same sheet (Boehme and Charton, 2005). Thus, in the present case, transparent conductor electrodes were printed in step two using PEDOT:PSS. These transparent electrodes provided necessary electrical contact between the biosensor (anode) and the PB display (cathode). Next, the biosensor graphite transducers were printed together with the text, which was mirror-imaged. The next step involved printing a white colour background layer to provide high contrast and facilitate reading

## Skin-patch self-powered electrochromic sensors can be fully screen-printed

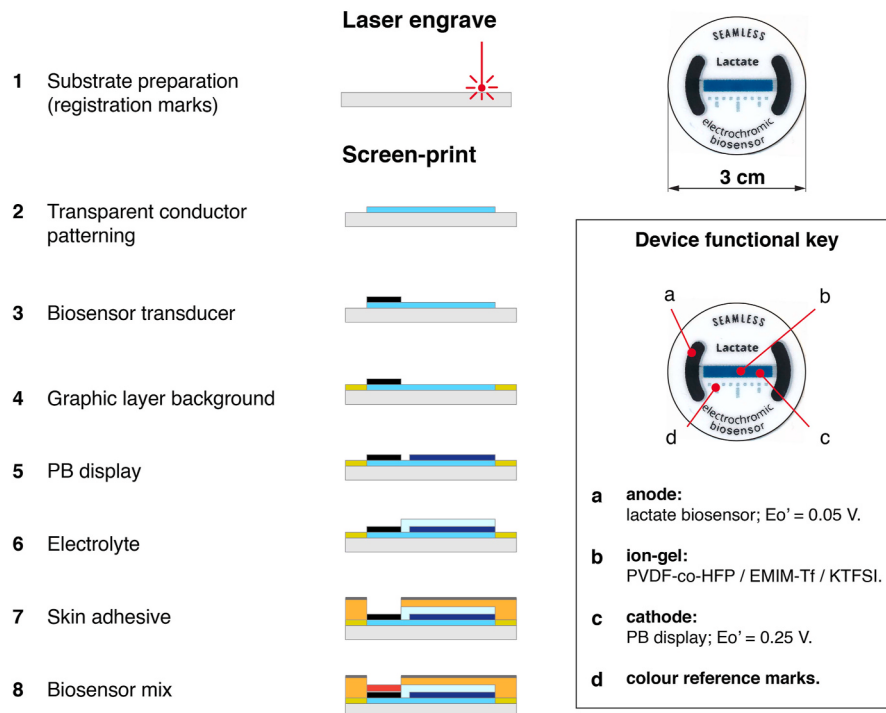


**Fig. 1.** Diagrammatic representation of the fabrication process and photographs from two different prototype versions. The inset highlights the function of the device various components.

both text and the display. The electrochromic PB display bars were printed next using an 80 durometer squeegee to ensure a thinner deposit. Standard screen-printing squeegees are made in lower durometer polyurethane rubber, typically sh70. The amount of PB deposited controls the device sensitivity and its response time; more material (i.e., thicker layers) may be used if higher concentrations need to be measured or if the biosensor has a very high current output. PB reference marks evenly distributed around the display (See device photographs in Fig. 1) served two purposes: first, they provided a colour reference for subsequent image data analysis and, second, they act as a spatial reference to determine more accurately the extent of the colour change along the longitudinal display axis. Fourth to be printed was a white dielectric that provided a background to the text and display, and facilitated reading out the results. The fifth, and last printed layer, was the electrolyte ion-gel, which had to be printed hot (60–70 °C) to prevent it from gelling on the screen. Three ion-gel layers were printed in the reported prototypes to reduce iR-drop losses due to the low electrolyte thickness (Aller-Pellitero et al., 2018). Note that the ion-gel covers the PB cathode and the gap between this, and the biosensor. The reason is to provide the cathode with a stable electrolyte environment irrespective of sweat pH and electrolyte composition and ensure a consistent response dependent on the analyte concentration only. Last, although an adhesive could be printed too, in our case, we used a non-woven, medical-grade PSA. This adhesive layer was laser-cut to expose the biosensors while protecting the ion-gel. Last, the complete devices were laser-cut, and the graphite electrodes functionalised as described above.

### 2.4. Instrumentation

PET substrates, electrodes and printed devices were cut using a 30 W CO<sub>2</sub> laser engraver by Epilog Mini 24 (Laser Project, ES). Electrochemical and spectroelectrochemical measurements were done using a

SPELEC UV-vis spectroelectrochemistry instrument (Metrohm-Dropsens, ES) controlled by DropView SPELEC software (version 3.0), installed on a PC running Windows 10.

### 2.5. Electrochemical measurements

Cyclic voltammetry (CV) was carried out using either a CHI600E (CH Instruments, Inc.) potentiostat and controlled by CHI600e software or a PalmSens 3 (PalmSens, NL) potentiostat controlled from a Windows 10-based laptop running PStrace 5.8 (PalmSens, NL). Solutions were degassed by bubbling argon whenever possible to remove oxygen, which can otherwise mask the PEDOT:PSS reduction wave. The open circuit potential was determined prior to any voltammetric experiments to ensure that cyclic voltammograms started at potential of zero current.

### 2.6. Image analysis device response analysis

Electrode images were captured using a Nikon D3300 camera, while images from the prototypes were captured using an iPhone. Image analysis was performed using Fiji (Schindelin et al., 2012), an ImageJ 1x distribution (Schneider et al., 2012). Best sensitivities were obtained from analysis of the red component of RGB images. A large area, ideally covering the whole electrode, was selected using the oval tool, and RGB information was obtained using the “RGB\_Measure\_Plus” free plugin. Note that the images shown in Figs. 3 and 4 have not been treated in any way.

## 3. Results & discussion

### 3.1. Spectroelectrochemical characterisation of screen-printed PB

The formulation and electrochemical response of the PB paste used here has been reported previously (Aller-Pellitero et al., 2019). Here, we

provide additional information regarding its spectroelectrochemical behavior (Kulesza et al., 1997; Mortimer and Reynolds, 2005). Fig. 2 shows cyclic voltammograms, UV–Vis spectra, and the corresponding voltabsorptograms at 680 nm of screen-printed 2.5 mm diameter disk PB and PEDOT:PSS electrodes. Fig. 2a shows the excellent electrochemical response of PB electrodes. The process around 0.2 V vs Ag/AgCl corresponds to the reversible reduction of PB to Prussian White, PW. The second process, found around 0.9 V vs Ag/AgCl, corresponds to the quasi-reversible oxidation of PB to Berlin Green, BG. However, because the device presented here works in a potential region between −0.1 and 0.3 V vs Ag/AgCl, the oxidation of PB to BG is not discussed. Fig. 2b corresponds to the absorption spectra, recorded in reflection mode, simultaneously with the cyclic voltammogram. The spectra show how light absorption decreases (reflectance increases) with potential as PB is bleached above 0.4 V vs Ag/AgCl to PW below 0.1 V vs Ag/AgCl. The voltabsorptograms depicted in Fig. 2c are the result of taking the time derivative of the absorption signal measured at 680 nm and represent the potentials where the colour changes take place, independently of background capacitive currents. This is a handy feature of voltabsorptograms, as they can pinpoint redox phenomena more clearly than cyclic voltammograms (Garoz-Ruiz et al., 2019). To facilitate the interpretation of the voltabsorptogram in the light of the CV, both curves have been coloured similarly in the figure. Orange and blue represent the forward and backward potential scan, respectively. Note that the data is expressed in terms of absorbance, so darker colours correspond to higher absorbance values and vice versa. The black trace in the figures represents the portion of the potential scan between the switching potential at the end of the backward scan, and the starting potential. The colour contrast ratio (CR) (Mortimer et al., 2015) of the PB electrode at 680 nm, determined as the ratio between the maximum and the minimum reflectance observed in the redox process between PB and PW, is 1.43. Note that some authors have claimed that for an electrochromic change to be noticed by the human eye, CR > 3–4 are recommended (Monk et al., 1995). Despite being close or even below this arbitrary limit, the PB/PW system is routinely (Jansod et al., 2020; Mortimer, 2011; Sekretaryova et al., 2014; Zhang et al., 2017, 2019) used in electrochromic devices due to its ease of preparation and use in many forms.

### 3.2. Spectroelectrochemical characterisation of screen-printed PEDOT:PSS

As Fig. 1 shows, the present device uses a transparent electrode. ITO coated PET sheets are commercially available in different grades of optical transmittance and electrical resistivity, and in sheet thicknesses down to 30 μm. However, these materials are costly and require additional processing compared to PEDOT:PSS, which can readily be applied by screen-printing. This is the reason why we chose PEDOT:PSS as our transparent electrode despite its relatively lower conductivity (ca. 400 Ω  $\square^{-1}$ ) compared to ITO on PET (ca. 60–75 Ω  $\square^{-1}$ ). Although the conductivity of PEDOT:PSS electrodes can be increased by printing thicker layers, this results in lower light transmission. Besides, PEDOT:PSS is known for its cathodic electrochromism (Andersson et al., 2007; Kim et al., 2020; Kumar et al., 1998; Mortimer and Reynolds, 2005). Given that our PB display is expected to work at low potentials, we studied the effect of PEDOT:PSS electrode thickness and applied potential on the optical properties of our cathode. The goal was to find the optimum balance between electronic conduction and film transparency, so that the colour change of the PB could be observed by sight unambiguously. This is extremely important because the colour contrast ratio our PEDOT:PSS printed electrodes is  $CR_{PEDOT:PSS} = 3.11$  at 685 nm which, compared to the  $CR_{PB/PW} = 1.43$  of the PB/PW system means that PEDOT:PSS is much more intensely coloured and may mask the colour change of our main electrochrome system, PB. In addition to the higher contrast, the PEDOT:PSS system is coloured more efficiently at 95% switch ( $183 \text{ cm}^2 \text{ C}^{-1}$ ) (Gaupp et al., 2002), than the PB system ( $143 \text{ cm}^2 \text{ C}^{-1}$ ), (Mortimer and Reynolds, 2005).

Fig. 2d shows the cyclic voltammetric response of the PEDOT:PSS electrodes used in the construction of the prototypes. The figure shows a large reduction signal starting at −0.5 V vs Ag/AgCl which, on analysis of the spectra presented in Fig. 2e, matches the voltabsorptograms in Fig. 2f. Although the apparent redox formal potential of this process is close to −750 mV vs Ag/AgCl, it is possible to observe some colour change at potentials starting at 0 V vs Ag/AgCl already. This is due to the structure of the polymer, which is likely to be composed of a mixture with different chain lengths. To check the suitability of PEDOT:PSS as transparent cathode for use in combination with the PB/PW system, we

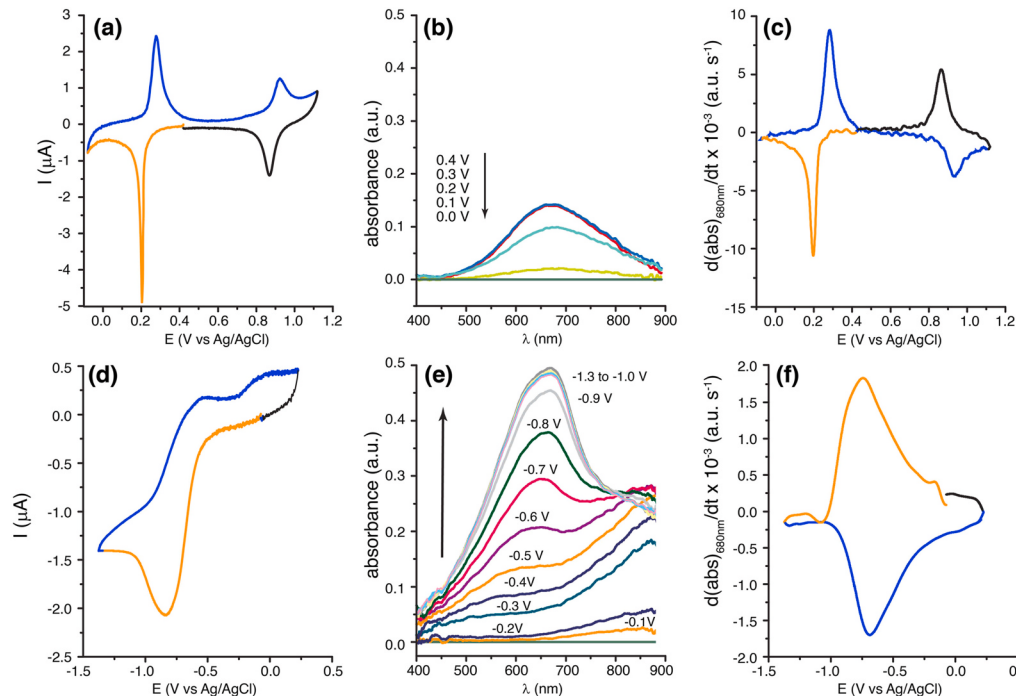


**Fig. 2.** (a) Cyclic voltammetry of a 3 mm PB disk on graphite in 0.1M KNO<sub>3</sub>. At 5 mV s<sup>-1</sup> (b) Absorption spectra collected during cyclic voltammetry (a). (c) voltabsorptogram of the PB/PW and PB/BG system combining information from 2a and 2b at 690 nm. (d) Cyclic voltammogram recorded at 5 mV s<sup>-1</sup> of a 2.5 mm PEDOT:PSS electrode in an Ar degassed 0.1 M KNO<sub>3</sub> solution. (e) Absorption spectra obtained from the PEDOT:PSS electrode during voltammetry (d), and (f) voltabsorptogram of PEDOT:PSS combining data from Fig. 2d and e at 680 nm.

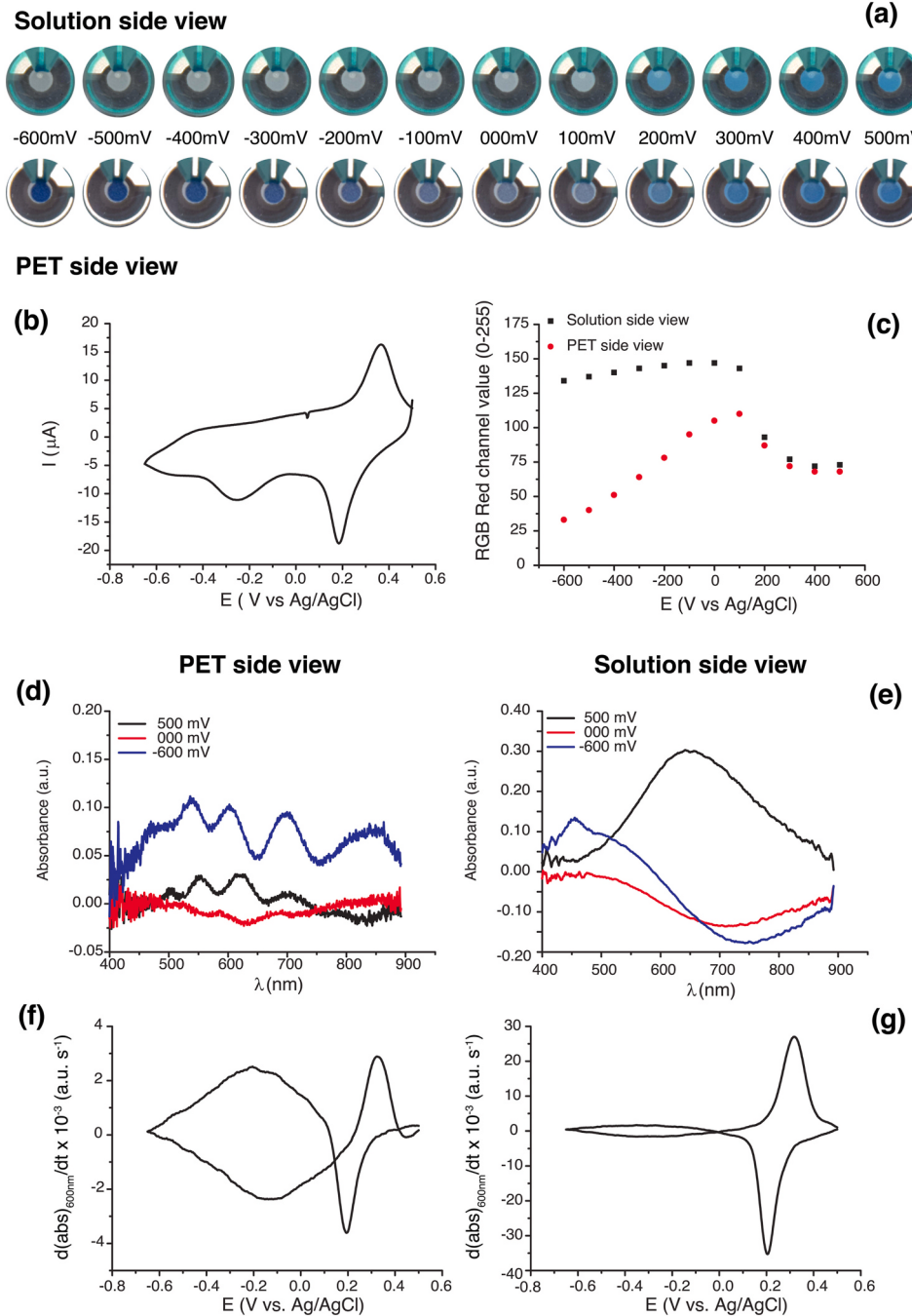


**Fig. 3.** (a) Solution and PET side view images of a PEDOT:PSS/PB on PET electrode during a (b) 10 mV s<sup>-1</sup> cyclic voltammetry in 0.1 M KNO<sub>3</sub> solution potentials are referenced versus an Ag/AgCl electrode. (c) Red channel value of the working electrode as a function of potential. Absorption spectra of the electrode taken from the (d) PET side and (e) solution side at three key potentials. Voltabsorptograms calculated from the (f) PET side and the (g) solution side spectra obtained in reflection mode during a 10 mV s<sup>-1</sup> cyclic voltammetry. (For interpretation of the references to colour in this figure legend, the reader is referred to the Web version of this article.)

printed disk electrodes featuring one, two, and three layers of PEDOT:PSS.

Consequently, the PB/PW transition should be visible through a PEDOT:PSS electrode. We used disk electrodes featuring one printed layer of PB on two printed layers of PEDOT:PSS to study this configuration, which was later used in the prototypes. These disk electrodes were prepared for cyclic voltammetry experiments on 100 micron-thick transparent PET substrates too. Fig. 3a shows a series of photographs from one of these electrodes, taken during the 10 mV s<sup>-1</sup> cyclic voltammetry in Ar-degassed 0.1M KCl shown in Fig. 3b. To facilitate image capture, these experiments were made in a standard 1 × 1 cm footprint spectrophotometry cuvette. The potential was scanned between 0.5 V and −0.6 V vs Ag/AgCl (0.1M LiCH<sub>3</sub>COO). The top image set was taken from the solution side of the electrode, whereas the image set below corresponds to the substrate (PET) side. Thus, the layers met by light in

the first case are PB/PEDOT:PSS, and in the second case PET/PEDOT:PSS/PB. This is why we find differences between both sets. First, in the solution-side view, we can clearly see the colour switching from blue to grey as potential passes the PB/PW reduction potential, around 150–200 mV. In the PET-side view, on the other hand, we observe two transitions because both PB and PEDOT:PSS are electrochromic. In spite of this, it is possible to observe the transition from PB to PW before the reduction of PEDOT:PSS masks the PW underneath it below −100 mV vs Ag/AgCl. Because image interpretation can be subjective, we have used ImageJ, an open-source image analysis software (Schindelin et al., 2012), to show how these electrodes behave and to establish the suitability of the system for the construction of the prototypes. We have selected a 1.5 mm diameter circular area within the working electrode and measured its RGB histogram. The RGB scale defines colours as the combination of red, blue and green, each ranging in a scale between

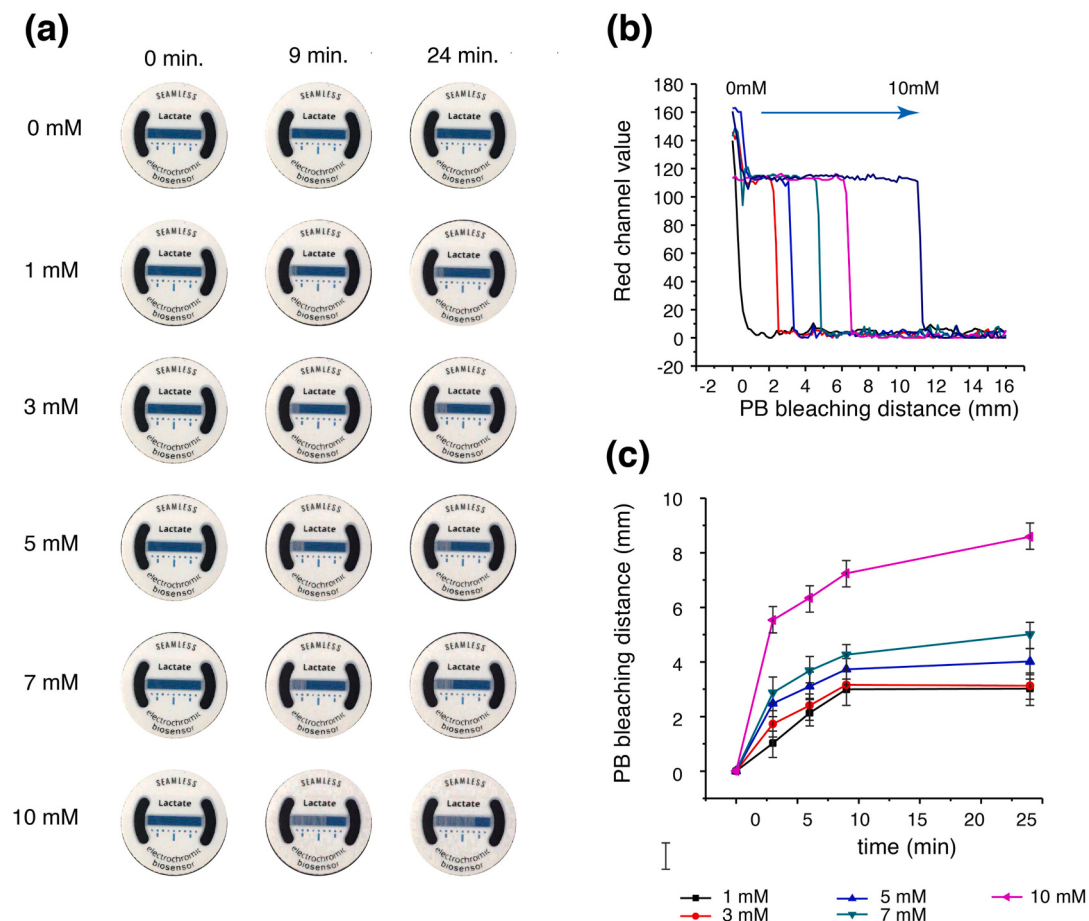


**Fig. 4.** a) Evolution of the display colour change as a function of lactate concentrations. (b) Red channel profile after 24 min in the presence of different lactate concentrations. (c) Transient evolution of the colour front from (b) as a function of lactate concentration. (For interpretation of the references to colour in this figure legend, the reader is referred to the Web version of this article.)

0 and 255. An RGB value of 0,0,0 denotes black, and 255,255,255 represents white. So the lower the value, the darker the tone. Fig. 3c shows the values corresponding to the red channel, which is the most sensitive in this case because it absorbs blue more strongly than the other channels. While quantification is easier from observation of the solution-side, it is also possible from the substrate side. In this case, the figure shows that it may be more difficult for potentials below  $-100$  mV because of the effect of PEDOT:PSS. However, as shown in Fig. 4a below, our lactate biosensor works above  $-100$  mV, so in the full system we can be sure that any colour changes will only be due to the PB/PW system, even if these are slightly dulled by the PEDOT:PSS layer. Additionally, we have also studied the system spectroelectrochemical response in reflection mode, under the same conditions.

Fig. 3d and e shows typical absorption spectra at the starting potential ( $+300$  mV), at the end potential ( $-600$  mV), and at an intermediate potential where the self-powered system is most likely to operate ( $0.00$  V). It is striking how different both sets of spectra are. While the solution side matches the spectra previously found for PB on graphite (Fig. 2b), the PET side spectra display distinct peaks around  $550$  nm,  $600$  nm,  $700$  nm and  $850$  nm. Of these, PB shows a broad peak between  $600$  and  $700$  nm, while PEDOT absorbs in a much broader range, so that the peaks around  $500$  nm and that at  $850$  nm may be attributed to PEDOT:PSS only. These two peaks do not appear at the solution-side spectra because the PB/PW coating, which is modifying  $3\ \mu\text{m}$   $\text{SiO}_2$ -ATO microparticles, is opaque. Last, Fig. 3f and g shows the corresponding voltabsorptograms at  $600$  nm. Both plots show two clear signals. A sharper one at higher potentials, corresponding to the PB/PW system, and a much broader one corresponding to PEDOT:PSS. The

relative magnitude of these signals in each case arises from the system construction. Thus, in the solution view voltabsorptogram (Fig. 3g), the PB signal dominates because the PEDOT:PSS layer is effectively hidden underneath. However, in the PET-side view voltabsorptogram, both the PB/PW and the PEDOT:PSS signals have comparable magnitudes. As we have seen, the deep blue colour of PEDOT:PSS dominates at potentials below  $-200$  mV vs Ag/AgCl.

### 3.3. Full device response

The self-powered device presented here is a galvanic system enabled by the low oxidation potential at the lactate biosensing anode and the higher reduction potential of the PB cathode. The operation has been fully described in the past (Aller Pellitero et al., 2018), but a summary will be given here for convenience. The presence of lactate activates the biosensor but, in contrast to conventional self-powered systems, the device internal resistance is a key design parameter that controls the extent of colour bleaching along the cathode. The electrons involved in the oxidation of lactate are relayed from the enzyme to the redox polymer, which passes them through the graphite electrode and the transparent electrode to the Prussian Blue, bleaching it. Due to the special geometry of the system, it is the PB closest to the anode that is bleached first. This changes the device internal resistance, increasing it, as the electrons need to cover a longer path before reaching new PB Fe (III) centres to reduce. In the solution side, this translates in an increasing  $iR$ -drop that is controlling the entire process. Thus, the cell potential,  $E_{\text{cell}} = E_{\text{cathode}} - E_{\text{anode}} - iR$ , which depends on analyte concentration, determines the length of the bleached area, while the biosensor

output current affects response time and colour front sharpness. In the present system, the system is known to generate open-circuit cell potentials, OCP, in the range of 0.5 V (Aller-Pellitero et al., 2020), and current densities in the range 100–300  $\mu\text{A cm}^{-2}$  depending on lactate concentration. Because both anode and cathode are connected by means of the transparent PEDOT:PSS electrode, it is not possible to measure the currents or the cell potentials generated in the presence of lactate. On the other hand, the device response was explored by measuring the bleaching colour of PB by image analysis in the presence of different lactate concentrations. Briefly, one of the graphite electrodes was modified using 5  $\mu\text{L}$  of the biosensor solution previously described. Filter papers were soaked in PBS-buffered (pH = 7) lactate solutions ranging from 1 mM to 13 mM. Once the biosensors were ready, the devices were placed on top of these soaked papers and pictures were taken every 3 min. The colour change of the display was subsequently analysed using imageJ. Fig. 5 summarizes the results obtained for the lactate biosensor. Fig. 5a shows photographs at the start, and then 9 and 24 min into the experiment. As expected, at higher lactate concentrations, a larger portion of the cathode was bleached (larger  $E_{cell}$ ), and the response was also faster (higher current).

Fig. 4b shows the red channel profile of the PB electrodes as a function of analyte concentration, at  $t = 24$  min. Low  $R$  (red channel) values are indicative of blue colour (red is absorbed), so as the electrode is bleached, the  $R$  value increases. Note that no colour change is observed in the absence of enzyme activity (absence of lactate), which indicates the selectivity of the device. The sharp drop in colour between the bleached and the coloured regions is striking. Previously, we had observed a blurry transition zone, due to ohmic drop effects (Aller-Pellitero et al., 2018). Even screen-printed systems showed such a blurry region (Aller-Pellitero et al., 2020). However, in this case the colour change is really sharp. We attribute this to two factors. First, the resistance of the PEDOT:PSS electrode, which is higher than the ITO (Aller-Pellitero et al., 2017) and the gold (Aller-Pellitero et al., 2020) electrodes used in previous device versions and, second, to the large biosensor area which is able to convert more lactate and deliver higher currents than the conventional, 3 mm diameter disk biosensor shown in Figure ESI 3.

Previously (Aller-Pellitero et al., 2017, 2020), we had used very highly conducting electrodes, so that the main  $iR$  losses appeared on the solution side (Aller-Pellitero et al., 2018). Previously used ITO on glass and gold paste electrodes presented resistances of  $<20 \Omega \square^{-1}$  and ca.  $0.1 \Omega \square^{-1}$ , respectively. In this case, on the other hand, The measured resistance of the 2-layer PEDOT:PSS electrodes is between 65 and 75  $\Omega$

$\square^{-1}$ . The total resistance of this transparent electrode, from the graphite anode to the far end of the cathode ranges from 350 to 550  $\Omega$ . This resistance further increases up to ca. 1 k $\Omega$  once the PB layer has been printed on top of the PEDOT:PSS (roughly  $300 \Omega \square^{-1}$ ). Although the device response is controlled by the ion-gel resistance (it is approximately 3 k $\Omega$  across the whole display), it is reasonable to think that the choice of electrode can also aid in controlling the device response, preventing the homogeneous distribution of potential across the entire electrode surface, as would happen with a conventional conductor. Fig. 4c shows the position of the colour change as a function of analyte concentration at different times. The data show how higher analyte concentrations lead to the higher biosensor currents responsible for the faster the response, in agreement with previous observations. The data also show that each concentration has an end point, which is also in agreement with our predictions for this kind of system, where colour is expected to change in a region such that the cell electromotive force (emf) is higher or equal to the system internal resistance. The system works in fact as a visual coulometer; in our experiment we are exposing the biosensor to large sample volumes, so the analyte concentration sets an emf for the system that can be assumed to remain constant throughout the experiment. This, combined with the resistance of the PEDOT:PSS electrode, explains why the colour edge appears so sharp. First, an  $E_{cell}$  is set that is only a function of lactate concentration. Next, the biosensor consumes all the PB (charge) within the region where  $iR$  drop compensates the cell  $\Delta V$ . This also explains the wider linear range shown in Fig. 5 in the self-powered devices compared to the amperometric biosensor (see ESI Fig. 3). The display length bleached at 10 mM lactate is approximately 12 mm. Considering the biosensor area and electrolyte resistance, and assuming a current output in the range of 300–350  $\mu\text{A}$ , We estimate an  $iR$  drop around 0.6–0.7 V, which is in agreement with our previous results for a similar system (Aller-Pellitero et al., 2020).

Last, Fig. 5 shows data corresponding to the current density measured at the biosensor (also shown in Figure ESI 2), and the position of the colour front measured at time 24 min. The coulometric data display almost twice as wide a linear range as the amperometric sensor.

Although the biosensors used in this work were first designed to work in whole blood (Punter-Villagrasa et al., 2015), and sweat lactate can be as high as 70 or 80 mM during exercise (Baker and Wolfe, 2020), we believe that the devices presented here demonstrate working principle of the proposed technology, and that they could be adapted to monitor lactate in sweat, or other analytes in different matrices. That, however, should necessarily involve changes in biosensor construction to fit the desired sensitivity.

#### 4. Conclusions

We have described the step-by-step construction and characterisation of a self-powered electrochromic sensor for the detection of sweat lactate. This device involves a transparent PEDOT:PSS electrode that connects a lactate biosensing anode, and a Prussian Blue electrochromic cathode. The biosensor is based on a classical construction involving lactate oxidase and an Osmium-based polyvinyl imidazole redox polymer, operates with an onset potential around 0 V vs Ag/AgCl and has a current output up to 350  $\mu\text{A cm}^{-2}$  in a lactate concentration range between 0 and 12 mM. The Prussian Blue cathode, on the other hand, presents a reduction onset potential around 0.3 V vs Ag/AgCl. The cathode contrast ration of 1.43 enables the colour change to be observed by the naked eye through the PEDOT:PSS electrode.

We have also assessed the importance of the choice of the transparent electrode material. In this case, we have used PEDOT:PSS because it makes for a more cost-effective and environmentally friendly production process than ITO. The suitability of PEDOT:PSS as a transparent electrode for this application has been studied in depth, considering both its electrical and spectroelectrochemical properties. PEDOT:PSS is a cathodic electrochrome turning from clear to deep blue at  $-0.9\text{V}$  vs Ag/

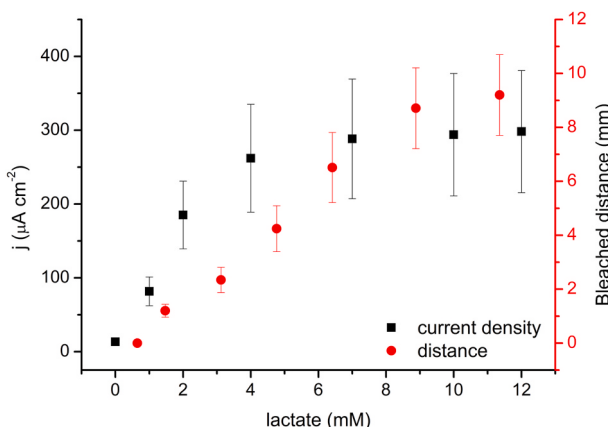


**Fig. 5.** Comparison between the amperometric biosensor response, expressed as current density (black squares, left axis) and the self-powered biosensor response, expressed as the position of the colour front, in mm away from the biosensor (red circles, right-hand axis). (For interpretation of the references to colour in this figure legend, the reader is referred to the Web version of this article.)

AgCl. However, the colouration process begins slightly below 0V vs Ag/AgCl, which may eventually mask the colour loss of PB and lead to wrong readings. However, the redox mediator used in the device ensures that the device does not operate below 0V, thus making PEDOT:PSS a suitable transparent electrode to work in combination with PB in this application.

Another critical element of this device is its ion-gel electrolyte, composed of PVDF-co-HFP, ionic liquid EMIM-Tf, and potassium triflate, which protects the PB display and provides an adequate chemical environment for its operation. This is important to prevent accidental bleaching of PB by species such as ascorbic or uric acid, which are known to reduce PB (Virbickas et al., 2019; Zloczewska et al., 2014). Also, this ion-gel protects PB from damaging neutral to basic pHs that may be found in certain samples. The potassium salt facilitates ion exchange with the sample medium and minimizes the junction potential at the aqueous sample-organic ion-gel interface. The printed ion-gel electrolyte resistance is close to  $600 \Omega \square^{-1}$ , and controls the device response.

The self-powered device has been studied using buffered lactate solutions. Although full response requires up to 24 min, the system reaches 85% of the final response within the first 10 min, making it suitable for use in applications such as endurance sport. The coulometric nature of the measurement extends the linear range up to 10 mM lactate, beyond the 4 mM linear range of the amperometric biosensors. It is believed that this is a combined effect of the cell potential established in the system between the display and the biosensor, and the relatively long reaction time. Considering the electrolyte resistance and the expected current output for the biosensor at 10–12 mM lactate, we can estimate a sensitivity involving the bleaching of 1 mm PB segments per mM unit of lactate.

The device presented in this work, with all its limitations, represents a step forward in the direction of more sustainable wearable biosensors. We have demonstrated that electrochromic materials can be successfully combined with biosensors to produce electrochemical devices performing three functions –energy generation, sensing, and information display– in a single electrochemical cell. Not only this, but we have also shown how to build it in a wearable form factor, with the biosensor facing one side, and the display facing the other. The presented device can be, after optimization of the transducers to fit the desired sensitivity, a promising approach for the non-invasive monitoring of target molecules excreted via perspiration.

#### CRediT authorship contribution statement

**Sara Santiago-Malagón:** Investigation, Formal analysis, Visualization. **Diego Río-Colín:** Investigation, Formal analysis, Visualization. **Haniyeh Azizkhani:** Investigation, Visualization. **Miguel Aller-Pellitero:** Conceptualization, Methodology, Writing - original draft, Writing - review & editing. **Gonzalo Guirado:** Resources, Writing - review & editing. **F. Javier del Campo:** Conceptualization, Methodology, Investigation, Formal analysis, Resources, Writing - original draft, Writing - review & editing, Supervision, Funding acquisition.

#### Declaration of competing interest

The authors declare that they have no known competing financial interests or personal relationships that could have appeared to influence the work reported in this paper.

#### Acknowledgements

MA is supported by FEDER funds managed by the Catalan Secretary of Universities and Research through project SEAMLESS (PROD-0000114; Enterprise and Knowledge, Industry Department, Generalitat de Catalunya). GG and SM also thanks the Agencia Estatal de Investigación (PID 2019-106171RB-100/AEI/10.13039/501100011033

project). The authors are grateful to Milliken for providing the electro-conductive powders (ECPs) featured in this work. Special thanks to our industrial partners in this project: Fernando Benito and Juan Echavarri, from Paymser, Ignasi Riera from Inkzar, and Joaquín Albert from Arista SG, for their invaluable guidance and support on printing materials, processes, and applications. Prof. Álvaro Colina (OrcID: 0000-0003-0339-356X), from the University of Burgos is gratefully acknowledged for his advice and discussions on spectroelectrochemical procedures.

#### Appendix A. Supplementary data

Supplementary data to this article can be found online at <https://doi.org/10.1016/j.bios.2020.112879>.

#### References

- Aller-Pellitero, M., Fremeau, J., Villa, R., Guirado, G., Lakard, B., Hihn, J.Y., del Campo, F.J., 2019. Sensor. Actuator. B Chem. 290, 591–597.
- Aller-Pellitero, M., Guimerà, A., Kitsara, M., Villa, R., Rubio, C., Lakard, B., Doche, M.-L., Hihn, J.-Y., Javier del Campo, F., 2017. Chem. Sci. 8, 1995–2002.
- Aller-Pellitero, M., Santiago-Malagón, S., Ruiz, J., Alonso, Y., Lakard, B., Hihn, J.Y., Guirado, G., del Campo, F.J., 2020. Sensor. Actuator. B Chem. 306, 127535.
- Aller-Pellitero, M., del Campo, F.J., 2019. Curr. Opin. Electrochem. 15, 66–72.
- Aller-Pellitero, M., Guimerà, A., Villa, R., del Campo, F.J., 2018. J. Phys. Chem. C 122, 2596–2607.
- Andersson, P., Forchheimer, R., Tehrani, P., Berggren, M., 2007. Adv. Funct. Mater. 17, 3074–3082.
- Baker, L.B., Wolfe, A.S., 2020. Physiological mechanisms determining eccrine sweat composition. Eur. J. Appl. Physiol. 120 (4), 719–752. Springer Berlin Heidelberg.
- Bandodkar, A.J.J., Lee, S.P.P., Huang, I., Li, W., Wang, S., Su, C.-J., Jeang, W.J.J., Hang, T., Mehta, S., Nyberg, N., Ghaffari, R., Rogers, J.A.A., Gutruf, P., Choi, J., Koo, J., Reeder, J.T., Tseng, R., Ghaffari, R., Rogers, J.A.A., 2020. Nat. Electron. 3, 554–562.
- Boehme, M., Charton, C., 2005. Surf. Coatings. Technol. 200, 932–935.
- Correia, D.M., Fernandes, L.C., Martins, P.M., García-Astrain, C., Costa, C.M., Reguera, J., Lanceros-Méndez, S., 2020. Adv. Funct. Mater. 30, 1909736.
- Dubal, D.P., Chodankar, N.R., Kim, D.-H., Gomez-Romero, P., 2018. Chem. Soc. Rev. 47, 2065–2129.
- Garoz-Ruiz, J., Perales-Rondon, J.V., Heras, A., Colina, A., 2019. Electroanalysis 31, 1254–1278.
- Gaupp, C.L., Welsh, D.M., Rauh, R.D., Reynolds, J.R., 2002. Chem. Mater. 14, 3964–3970.
- Grattieri, M., Minteer, S.D., 2018. ACS Sens. 3, 44–53.
- Heikenfeld, J., Jajack, A., Rogers, J., Gutruf, P., Tian, L., Pan, T., Li, R., Khine, M., Kim, J., Wang, J., Kim, J., 2018. Lab Chip 18, 217–248.
- Huang, L., Chen, J., Yu, Z., Tang, D., 2020. Anal. Chem. 92, 2809–2814.
- Jansod, S., Cherubini, T., Soda, Y., Bakker, E., 2020. Anal. Chem. 92, 9138–9145.
- Jin, X., Bandodkar, A.J., Fratus, M., Asadpour, R., Rogers, J.A., Alam, M.A., 2020. Biosens. Bioelectron. 168, 112493.
- Kim, D.-H., Lu, N., Ma, R., Kim, Y.-S., Kim, R.-H., Wang, S., Wu, J., Won, S.M., Tao, H., Islam, A., Coleman, T., Rogers, J.A., 2011. Science 333, 838–843.
- Kim, J., Campbell, A.S., de Ávila, B.E.-F., Wang, J., 2019. Nat. Biotechnol. 37, 389–406.
- Kim, J., Rémond, M., Kim, D., Jang, H., Kim, E., 2020. Adv. Mater. Technol. 5, 1–22.
- Kulesza, P.J.P.J., Zamponi, S., Malik, M.A.A.M.A., Miecznikowski, K., Berrettoni, M., Marassi, R., 1997. J. Solid State Electrochem. 1, 88–93.
- Kumar, A., Welsh, D.M., Morvant, M.C., Pioux, F., Abboud, K.A., Reynolds, J.R., 1998. Chem. Mater. 10, 896–902.
- Liana, D.D., Raguse, B., Gooding, J.J., Chow, E., 2015. ACS Appl. Mater. Interfaces 7, 19201–19209.
- Liu, H., Crooks, R.M., 2012. Anal. Chem. 84, 2528–2532.
- Mendes-Felipe, C., Oliveira, J., Etxebarria, I., Vilas-Vilela, J.L., Lanceros-Mendez, S., 2019. Adv. Mater. Technol. 4, 1800618.
- Monk, P.M.S., Mortimer, R.J., Rosseinsky, D.R., 1995. Electrochromism Fundamentals and Applications, first ed. VCH, Weinheim.
- Mortimer, R.J., 2011. Annu. Rev. Mater. Res. 41, 241–268.
- Mortimer, R.J., Reynolds, J.R., 2005. J. Mater. Chem. 15, 2226–2233.
- Mortimer, R.J., Rosseinsky, D.R., Monk, P.M.S., 2015. Electrochromic Materials and Devices, Electrochromic Materials and Devices.
- Oliveira, J., Correia, V., Castro, H., Martins, P., Lanceros-Mendez, S., 2018. Addit. Manuf. 21, 269–283.
- Ortega, L., Llorella, A., Esquivel, J.P., Sabaté, N., 2019. Microsystems Nanoeng 5, 3.
- Popov, A., Brasiunas, B., Mikoliunaite, L., Bagzdilas, G., Ramanavicius, A., Ramanaviciene, A., 2019. Polymer 172, 133–141.
- Punter-Villagrassa, J., Paez-Aviles, C., Colomer-Farrarons, J., Lopez-Sanchez, J., Juanola-Feliu, E., Miribel-Catala, P., Cid, J., Kitsara, M., Aller-Pellitero, M., Sabaté, N., Del Campo, F.J., Rodriguez-Villarreal, I., 2015. A portable point-of-care device for multi-parametric diabetes mellitus analysis. In: IECON 2015 - 41st Annual Conference of the IEEE Industrial Electronics Society, pp. 1252–1257.
- Rose, D., Ratterman, M., Griffin, D., Hou, L., Kelley-Loughnane, N., Naik, R., Hagen, J., Papautsky, I., Heikenfeld, J., 2014. IEEE Trans. Biomed. Eng. 9294, 1.
- Ruff, A., 2017. Curr. Opin. Electrochem. 5, 66–73.

- Santiago, S., Muñoz-Berbel, X., Guirado, G., 2020. *J. Mol. Liq.* 318, 114033.
- Schindelin, J., Arganda-Carreras, I., Frise, E., Kaynig, V., Longair, M., Pietzsch, T., Preibisch, S., Rueden, C., Saalfeld, S., Schmid, B., Tinevez, J.-Y., White, D.J., Hartenstein, V., Eliceiri, K., Tomancak, P., Cardona, A., 2012. *Nat. Methods* 9, 676–682.
- Schneider, C.A., Rasband, W.S., Eliceiri, K.W., 2012. *Nat. Methods* 9, 671–675.
- Sekretaryova, A.N., Beni, V., Eriksson, M., Karyakin, A.A., Turner, A.P.F., Vagin, M.Y., 2014. *Anal. Chem.* 86, 9540–9547.
- Singh, R., Tharion, J., Murugan, S., Kumar, A., 2017. *ACS Appl. Mater. Interfaces* 9, 19427–19435.
- Virbickas, P., Valiūnienė, A., Kavaliauskaitė, G., Ramanavicius, A., 2019. *J. Electrochem. Soc.* 166, B927–B932.
- Windmiller, J.R., Bandodkar, A.J., Valdés-Ramírez, G., Parkhomovsky, S., Martínez, A.G., Wang, J., 2012. *Chem. Commun.* 48, 6794.
- Xiao, X., Xia, H.Q., Wu, R., Bai, L., Yan, L., Magner, E., Cosnier, S., Lojou, E., Zhu, Z., Liu, A., 2019. *Chem. Rev.* 119, 9509–9558.
- Yu, Z., Cai, G., Ren, R., Tang, D., 2018. *Analyst* 143, 2992–2996.
- Yu, Z., Cai, G., Tong, P., Tang, D., 2019. *ACS Sens.* 4, 2272–2276.
- Zhang, F., Cai, T., Ma, L., Zhan, L., Liu, H., 2017. *Sensors* 17, 276.
- Zhang, X., Lazenby, R.A., Wu, Y., White, R.J., 2019. *Anal. Chem.* 91, 11467–11473.
- Złoczewska, A., Celebanska, A., Szot, K., Tomaszevska, D., Opallo, M., Jönsson-Niedziolka, M., 2014. *Biosens. Bioelectron.* 54, 455–461.